Titanium oxynitride coated graphite paper electrodes for light-weight supercapacitors

Ananthakumar Ramadoss[1,2,*] (iD), Nilimapriyadarsini Swain[2], Gobi Saravanan[3],
Sohaila Z. Noby[4], K. Kirubavathi[1], Lukas Schmidt-Mende[4], and K. Selvaraju[1,*]

[1] *Department of Physics, Government Arts College (Affiliated to Bharathidasan University), Ariyalur 621713, India*

[2] *Laboratory for Advanced Research in Polymeric Materials (LARPM), School for Advanced Research in Polymers (SARP), Central Institute of Petrohemicals Engineering and Technology (CIPET), Bhubaneswar 751024, India*

[3] *Centre for Nanoscience and Nanotechnology, Sathyabama University, Chennai 600119, India*

[4] *Department of Physics, University of Konstanz, Universitätsstr. 10, POB-680, 78457 Konstanz, Germany*

ABSTRACT

The rapid development of smart electronics devices has stimulated intensive research on flexible supercapacitors with high mechanical tolerance and energy density. Up to date, most of the asymmetric devices are fabricated using carbon-based materials as negative electrode materials. However, the lower capacitance of carbon-based materials limited its applicability widely. Also, the device unavoidably carries unnecessary mass and volume, leads to poor contact and performance to repeated bending of devices, and occupies more space in the electronics devices. Herein, we prepared flexible, light-weight, and thin graphite paper current collectors to fabricate flexible supercapacitors. Further, the titanium oxynitride (TiO_xN_y) coatings were deposited by DC magnetron sputtering over a flexible and light-weight graphite substrate as a potential negative electrode. The presence of nitrogen content in transition metal oxynitrides adds wettability to the material; hence more electrolyte ions get adsorps onto the surface of the electrode owing to their hydrophilic nature. The resultant TiO_xN_y/graphite electrode exhibited a high areal capacitance of 62 mF cm^{-2} and also showed 100% capacitance retention even after 1500 GCD cycles. The results of a series of tests indicated that the flexible electrode has better capacitive performance, suggesting that as-prepared film is a favorable candidate for light-weight and flexible supercapacitors.

Address correspondence to E-mail: ananth@larpm.in; selsphy@yahoo.com

1 Introduction

In the modern phase of energy evolution, we are witnessing the day-to-day life of electronics world. The usability and demand for miniature, portable, and light-weight gadgets have directed the way to change the face of modern electronic devices. Consequently, significant efforts are being made to enhance the performance of energy storage devices and developing new concepts and novel materials for these devices [1, 2]. This trend in the development of energy storage devices moves forward towards the successful implantation of light-weight, conductive, and efficient charge storage materials into a flexible frame that results in the expansion of flexible supercapacitors [3–6]. These devices can afford high flexibility, remarkable storage capability, simplified chemistry than batteries. Additionally, good electrochemical parameters such as capacitance, power density and energy density are also reflected in their performance. Hence it is challenging to develop such devices showing better performance than the existing energy storage devices [5]. Typically, to develop the flexible current collector, substrates like fibers, carbon-based cloths, metal foils, tapes, and wires can be used to support the electroactive materials [7–11].

In order to expand electrochemical performances, several strategies have been adopted [12–19]. For example, metal nitrides have become preferable, in recent years, as suitable electroactive materials in supercapacitors owing to their excellent electrical conductivity. Their conductivity is comparable to that of metals and hence they are helpful in the effective collection and fast transport of charges. Even though the metal nitride-based supercapacitors are auspicious, their perspective is limited due to their short cycle-life and poor rate performance. In this study, we have fabricated titanium oxynitride (TiO_xN_y) based electrodes for flexible supercapacitors by taking both the advantages of nitrogen and oxygen. The TiO_xN_y are novel candidates due to their salient features such as excellent electrical conductivity, large voltage window, high thermal, mechanical and chemical stability, large surface area, structural tailorability, hydrophilic nature, which make them superior over their nitride counterparts [20–22]. Though the pristine TiO_2 and TiN have good electrochemical performance, they still suffer from poor intrinsic conductivity and rate capability, which can be rectified by introducing nitride or oxide groups

[23, 24]. Lee et al. [25] fabricated the hierarchically structured TiO_xN_{1-x} electrode using the nitridized approach and delivered a maximum specific capacitance of 93.4 (h-TiO_xN_{1-x}) and 95.6 (n-TiO_xN_{1-x}) F g^{-1} at 2 mV s^{-1}. Similarly, Yan et al. [26] prepared the TiON nanoparticles over the CNT surface via annealing treatment under the ammonia atmosphere. The hybrid electrode showed the specific capacitance of 187 F g^{-1} at 0.5 A g^{-1} with lesser long term stability of 80% within 1000 cycles. Further, the flexible free-standing TiOxNy sheets were synthesized by the nitridation of titanate fibers and reported by Chen et al. [20]. The freestanding electrode showed a gravimetric capacitance of 120.9 F g^{-1} at 1.25 A g^{-1}. However, the electrochemical performance has not attained a higher level and also metal oxynitrides have been rarely examined for supercapacitors. With these in mind, herein, we demonstrate the fabrication of TiO_xN_y based flexible electrodes and their characterizations using various physicochemical techniques. The resulting electrodes delivered a areal capacitance of 62 mF cm^{-2} along with 100% withholding capacity after 1500 cycles, thus demonstrating better electrochemical behavior.

2 Experimental details

2.1 Materials

Potassium hydroxide (KOH), and sulfuric acid (H_2SO_4) in this experiment were used as analytical reagents and were purchased from Hi-media, India. Titanium (Ti, 99.99%) target was purchased from Itasco, South Korea. A graphite sheet used as a current collector was obtained from the M/s Fluidline Industrial Packing & Seals, India. The flexible graphite paper electrode (1 cm × 3 cm) was prepared via a facile mechanical exfoliation process using Kapton tape by applying hand force. The surface was then modified with sulfuric acid treatment. This process removed impurity, enhanced the hydrophilic interactions and induce hydrogen bonding for better adhesion. The wettability nature of the electrode influences the faster ion penetration towards the electrode surface, leading to better electrochemical performance. All chemicals were used as received without further purification.

3 Preparation of titanium oxynitride (TiO_xN_y) thin films

Binder-free titanium oxynitride thin films on flexible graphite/Kapton substrate were deposited by a reactive direct current (DC) magnetron sputtering (PLASSYS, FRANCE, MP 300) from the titanium target. Argon, oxygen, and nitrogen with purities of 99.999% were used as sputtering gas and reactive gas, respectively, for TiO_xN_y thin film coating. The deposition was performed after the sputtered chamber base pressure reached 3×10^{-6} mbar with the help of turbomolecular and rotary pumps. The target and substrate were pre-treated by Ar plasma for 10 min to clean their surfaces before the coating and improve the adhesion of the film. Deposition parameters such as target-to-substrate distance, temperature, and sputtering power were fixed at 50 mm, 450 °C, and 100 W, respectively. The deposition of TiO_xN_y thin film was achieved at a working pressure of 7.8×10^{-3} mbar and using 12 sccm of argon gas and 3 sccm mixture of oxygen and nitrogen gases for 120 min. The effective area and thickness of the deposited coatings was 1 cm^2 and $\sim$ 1 μm, respectively.

4 Physicochemical characterization of TiO_xN_y/graphite electrode

The crystal structure of the TiO_xN_y/graphite electrode was identified by X-ray diffraction (XRD) patterns performed using XRD-7000 L, Shimadzu, Japan. Raman analysis was performed using Micro-Raman Spectrometer, HORIBA France, LABRAM HR Evolution. Field emission scanning electron microscopy (FE-SEM, Zeiss Cross Beam 1540XB) studies was used to analyze the morphology of the electroactive material. The elemental composition of the film was obtained from energy dispersive analysis of the X-ray (EDAX) unit attached to the FE-SEM. X-ray photoelectron spectroscopy (XPS) analyzed the chemical compositions of the deposited TiO_xN_y/-graphite films by XPS, PHI 5000 Versa Probe III.

5 Electrochemical measurements

The electrochemical performance of as-deposited films was studied by cyclic voltammetry (CV), galvanostatic charge-discharge (GCD) curves, and electrochemical impedance spectroscopy (EIS) tests. The TiO_xN_y/graphite as a negative electrode was examined in 1 M KOH electrolyte using a typical three-electrode system considering platinum (Pt) wire as counter electrode and Hg/HgO as a reference electrode. The electrochemical test of all the samples was performed at room temperature using an electrochemical workstation (PMC1000, PARSTAT, USA). The geometrical area of the as-prepared electrode is 1 cm^2. The areal capacitance (C_a, F cm^{-2}), was calculated from the CV and GCD curves [27]:

$$C_a = \frac{\int i dV}{2SA\Delta V} \tag{1}$$

$$C_a = \frac{It}{A\Delta V} \tag{2}$$

where $\int i dV$ (A), S (mV s^{-1}), A (cm^2), $\Delta V(V)$ and I (A) refer to the integral area under the CV curve, the scan rate, the effective area of the electrode, the potential window during the discharge process and the discharge current, respectively and t is the discharge time.

6 Results and discussion

The fabrication of TiO_xN_y/graphite electrode is schematically illustrated in Fig. 1. A flexible, light-weight graphite/Kapton current collector electrode is initially prepared via a simple exfoliation process. To realize the hydrophilic nature of the graphite surface, the sample was then subjected to chemical treatment using sulfuric acid. Lastly, the titanium oxynitride thin films were fabricated onto the flexible current collector using a reactive DC-magnetron sputtering method. The digital images of as-prepared electrodes are shown in Fig. 1, which confirm the light-weight, flexible and twistable characteristics of the TiO_xN_y/graphite electrode.
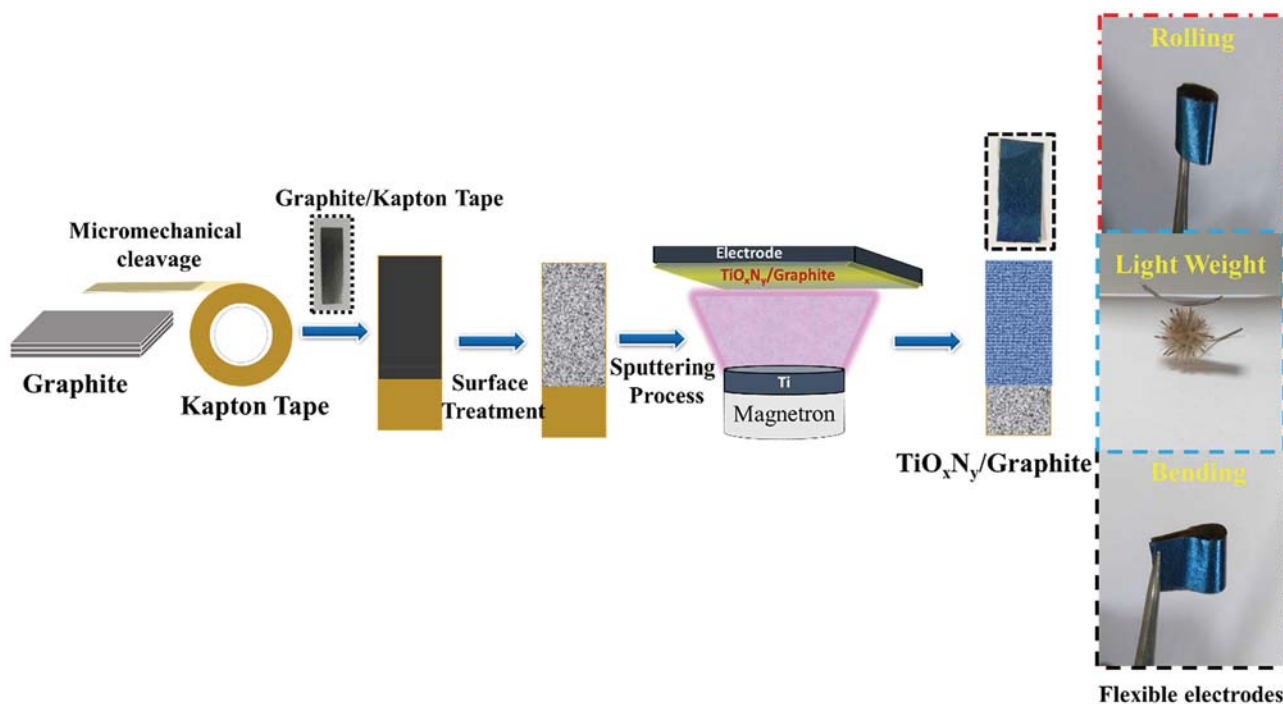
Fig. 1 Schematic diagram of preparation process of flexible titanium oxynitride/graphite electrode

7 Film structure, morphology and composition of the deposited film

To avoid the substrate peaks and confirm the phase formation, TiO_xN_y film was deposited on a glass substrate and studied by X-Ray diffraction. The typical XRD pattern of TiO_xN_y /graphite electrode is presented in Fig. 2a. As can be seen, the three diffraction peaks obtained at 36.6, 42.8, and 78° were attributed to (111), (200), and (222) planes of TiO_xN_y material, respectively [28, 29]. Further, the structure of the as-prepared electroactive material is examined by Raman spectroscopy (as displayed in Fig. 2b). The broad peaks at ~ 215, ~ 295 and ~ 560 cm^{-1} belong to the TiO_xN_y phase [30].

The FE-SEM images in Fig. 2c–d elucidate the TiO_xN_y uniform coverage of TiO_xN_y on the graphite paper appears as a relatively rough, irregular and loose architectural surface. The elemental composition of the as-prepared flexible electrode was determined by energy dispersive spectroscopy (EDS). From the EDS spectrum (Fig. 3a), it can be found that the presence of the Ti, O, and N elements mainly arises from the TiO_xN_y and C arises from the current collector. Furthermore, the distribution of these elements were analyzed by selected area elemental mapping of Ti, O, N and C (Fig. 3b–f), which shows

the homogeneous distribution throughout the TiO_xN_y/graphite surface. The presence of a noticeable amount of oxygen and nitrogen suggests the formation of titanium oxynitride, which is in good agreement with the results attained by the XPS survey spectrum.

The TiO_xN_y/graphite paper electrode was further explored in detail by XPS to demonstrate the formation of the oxynitride nanostructure. The survey spectrum (Fig. 4a) exhibited Ti, O, N, and C elements in TiO_xN_y/graphite paper electrode. The core level of Ti 2p, O 1s, and N 1s high-resolution spectra and their Gaussian curve fitting results are presented in Fig. 4a. The core level of Ti 2p spectra (Fig. 4b) of TiO_xN_y/graphite paper electrode is identified to be two doublet peaks Ti 2p$_{3/2,}$ and Ti 2p$_{1/2}$. The Ti 2p$_{3/2}$ peaks were decomposed into three sub-peaks at 455.6, 457.5, and 459.3 eV, corresponding to Ti–N, Ti–N–O, and Ti–O bonding of the TiO_xN_y phases, respectively. Similarly, Ti 2p$_{1/2}$ peaks were also decomposed into two sub-peaks at 461.5 and 464.9 eV, corresponding to the TiN and Ti–O states, respectively confirming the formation of titanium oxynitride films [29, 31–35]. The O 1s spectrum (Fig. 4c) divided into two peaks at 530.9 and 532.6 eV can be ascribed to TiO_2 and Ti–N–O components, respectively [29, 35, 36]. The N 1s XPS spectrum
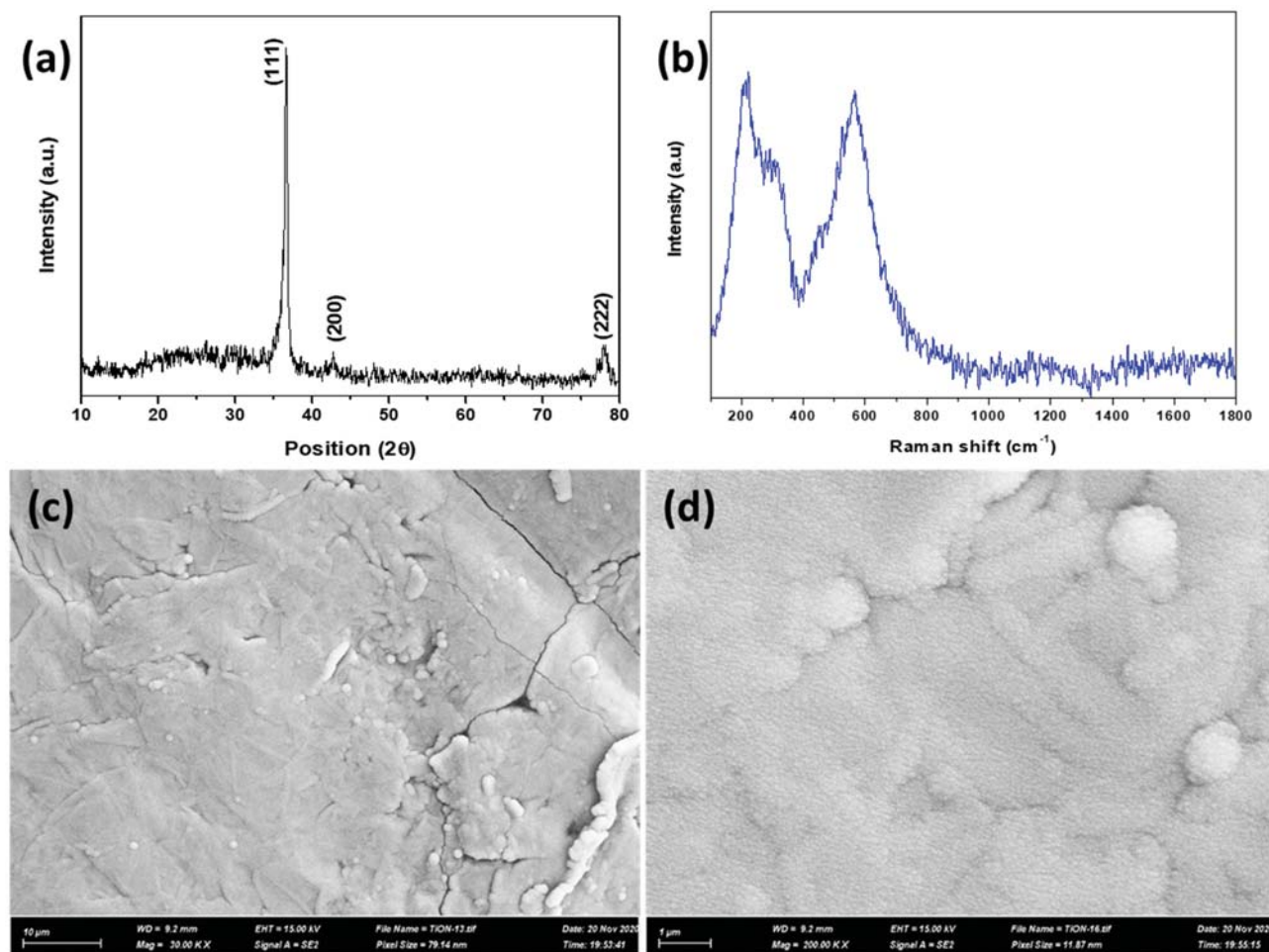
Fig. 2 Physiochemical characterizations of TiO_xN_y/graphite flexible electrode. **a** XRD pattern, **b** Raman spectrum and **c, d** FE-SEM images

(Fig. 4d) was deconvoluted with three kinds of nitrogen peaks at 396.4, 397.1, and 399.0 eV that can be assigned to the TiN, Ti–N–O, and absorbed N, respectively [29, 35, 36]. In short, the as-prepared electroactive material with oxygen and nitrogen content is expected to be an excellent negative electrode.

8 Electrochemical characterization

The electrochemical behavior of TiO_xN_y was validated using the three-electrode setup in an aqueous 1 M KOH solution. Figure 5a indicates the cyclic voltammograms (CVs) of TiO_xN_y acquired in the potential range of 0–1.1 V and were conducted at various scan rates from 5 mV s^{-1} to 125 mV s^{-1}. A quasi-rectangular shape was observed throughout the entire potential range, attributed to the electrodes pseudocapacitive nature. The quasi-rectangular shape was maintained even at high scan rates without any severe distortion, implying the electrodes' good capacitive behavior. The specific capacitances of TiO_xN_y as a function of scan rate are presented in Fig. 5b. The prepared electrode exhibited a maximum areal capacitance of 86 mF cm^{-2} at 5 mV s^{-1}. With an increase in the scan rate, a lower specific capacitance value was observed due to the slower ions diffusion and/or migration onto the surface in a certain short time frame [37].

Further, to evaluate the electrode, the GCD cycles (Fig. 5c) were performed from 1 mA cm^{-2} to 10 mA cm^{-2}; a little deviation in the symmetric shape indicates the pseudocapacitive behaviors as well as the good reversibility of the as-fabricated electrode. The calculated areal capacitance of TiO_xN_y electrode is 62
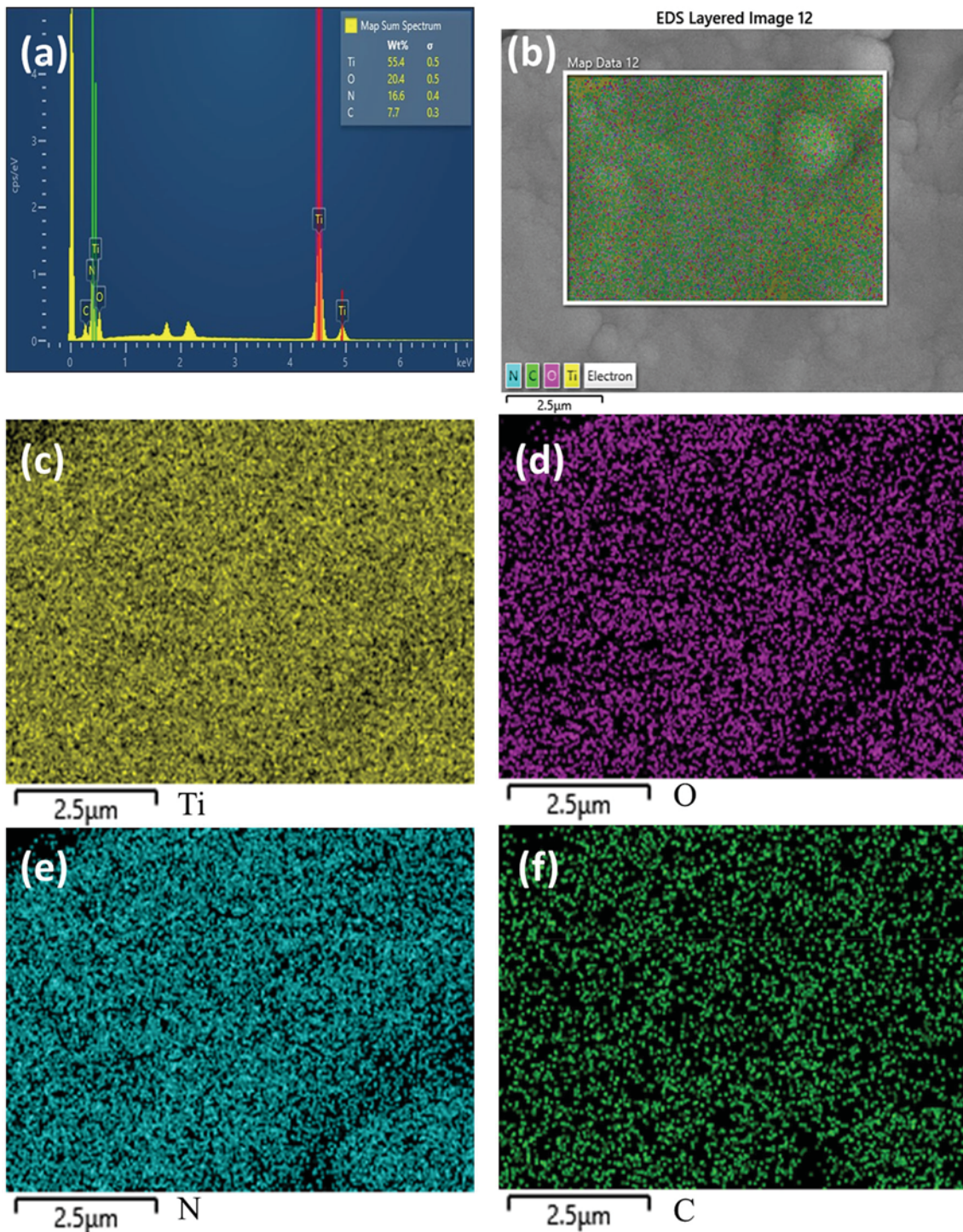
Fig. 3 a EDS spectrum and **b–f** elemental mapping images of Ti, O, N and C

mF cm^{-2} at 1 mA cm^{-2} (shown in Fig. 5d). Reduced specific capacitance was observed at a higher current density due to the limited numbers of electrolyte ions diffusion and migration resulting in the low utilization of electroactive TiO$_x$N$_y$ materials [20]. Further, the present result is comparable and higher than the previously reported metal nitride electrodes including titanium nitride films (8.8 mF cm^{-2} at 100 mV s^{-1} [38]; 10.9 mF cm^{-2} at 100 mV s^{-1} [39]; 26.9 mF cm^{-2} at 1 mA cm^{-2}[40]), vanadium nitride films (22.8 mF
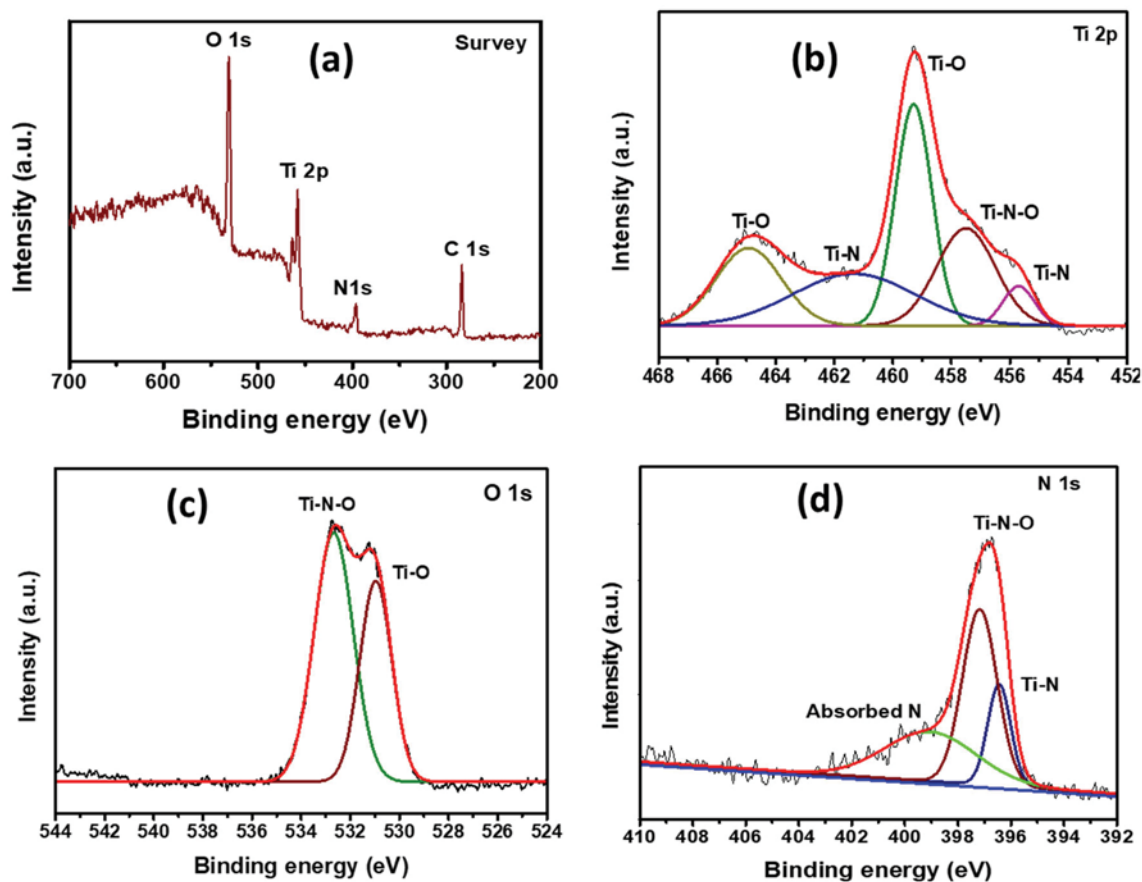
Fig. 4 XPS spectra with deconvolution curves of the TiO$_x$N$_y$/graphite films. **a** Survey, **b** Ti 2p, **c** O 1s and **d** N 1s

cm^{-2} at 100 mV s^{-1} [41]), molybdenum nitride film (52.4 mF cm^{-2} at 10 mV s^{-1} [42]), niobium nitride films (37.0 mF cm^{-2} at 0.2 mA cm^{-2} [43]; 39.6 mF cm^{-2} at 1 mA cm^{-2} [40]), chromium nitride film (31.3 mF cm^{-2} at 1.0 mA cm^{-2})[44], and titanium niobium nitride (59.3 mF cm^{-2} at 1 mA cm^{-2})[40].

Further, cycling stability was performed at 2 mA cm^{-2} for 1500 repeated cycles to evaluate the electrode performance. Almost 100% capacitance retention (Fig. 6a) was observed even after 1500 operation cycles, demonstrating the better electrochemical behavior of the flexible electrode. Moreover, the inset of Fig. 6a shows the symmetric charge/discharge characteristics throughout the cycles. Finally, the electrochemical impedance spectroscopy (EIS) was performed to determine the conductive properties of electrode materials with a frequency range of 0.01 Hz to 100 kHz. The measured and fitted (ZSimpWin software) Nyquist plots are shown in Fig. 6b. The fitted equivalent circuits (R(Q(RW))(CR): inset of Fig. 6b) consists of various elements including

solution resistance (R_s), charge transfer resistance (R_{ct}), a constant phase element (CPE), Warburg impedance (Z_W), capacitance (C) and surface film resistance (R_f). From Fig. 6b, it has been observed that the TiO$_x$N$_y$ electrode displays a slightly larger solution resistance (R_s) value (14.26 Ω) than that of the EIS before the test (10.57 Ω). The larger resistance observed might be due to the long operation cycles, heat generation, and some material degradation. However, the nominal charge transfer resistance [R_{ct}: 0.01322 (before cycle) and 0.01799 (after cycle)] in the high-frequency region indicated the better electrical conductivity of the electrode even after the cycling test.

The better supercapacitive performance of the as-prepared TiO$_x$N$_y$/graphite electrode can be attributed to various factors. (i) The uniformity and better adhesion of the coating over the flexible substrate lead to low interfacial resistance and a fast charge transfer rate. (ii) The binder-free direct deposition of the active materials over the current collectors avoids
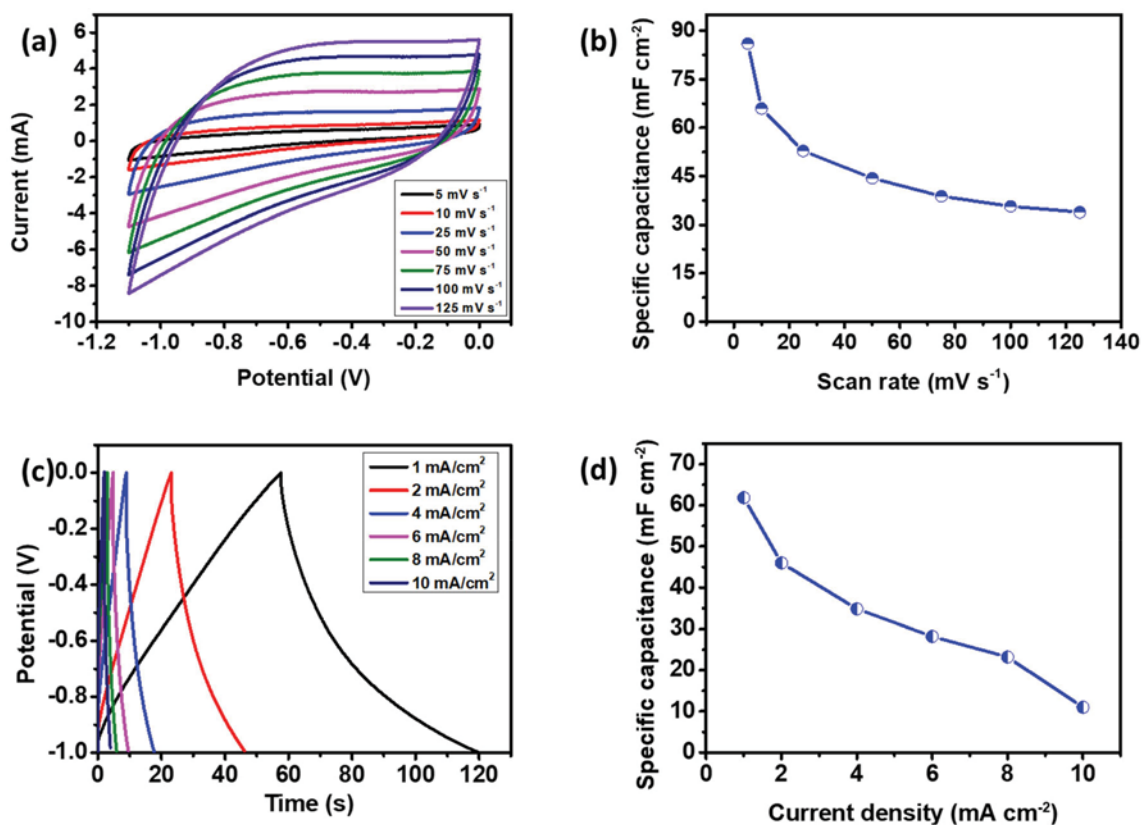
Fig. 5 **a** CV curves and **b** specific capacitance with varying scan rates **c** GCD curves and **d** specific capacitance with varying current densities of TiO_xN_y/graphite electrode
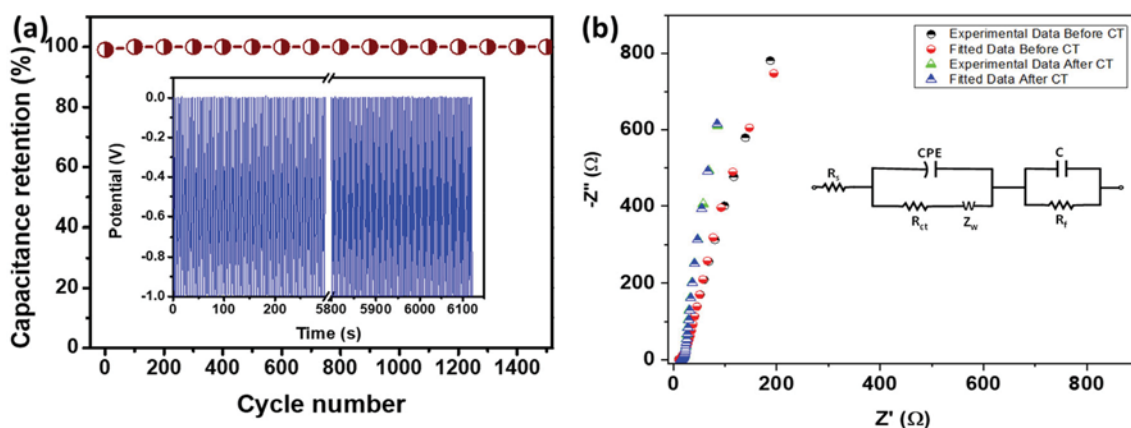

Fig. 6 **a** Cycling performance of TiO_xN_y/graphite electrode; inset is the charge/discharge cycles. **b** Nyquist plot of TiO_xN_y/graphite electrode before and after 1500 cycles; Inset is the equivalent circuit

using polymeric binders and conductive additives. (iii) Synergetic effect of Ti, O and N offer favorable electrical conductivity and wettability endorsing a fast redox reaction within the electrolyte for the enhanced charge storage. Owing to all these factors, the well interconnected thin-film strategy of TiO_xN_y/graphite proves to be suitable for miniature and flexible energy storage devices.

9 Conclusions

The recent advances on flexible electronic devices are paid more attention towards the utilization of metal oxynitrides. The available merits of nanostructured oxynitrides are certainly beneficial while designing the supercapacitor electrodes. Due to the wide variety of synthesis methods available, a well interconnected thin-film strategy is very important while deciding the synthesis approach. So herewith, titanium oxynitride coated thin film was obtained by DC magnetron sputtering technique. The as-obtained light-weight and flexible titanium oxynitride electrodes delivered a specific capacitance of 62 mF cm^{-2} at a current density of 1 mA cm^{-2}. Furthermore, the as-acquired electrode demonstrated 100% capacitance retention after 1500 cycles. Comprising with the good electrochemical performance, the light-weight, flexible, and binder-free approach of the titanium oxynitride electrode makes it more suitable for light-weight and miniature electronic devices. Thus, proving that it could be a better choice for upcoming light-weight energy storage devices.

Author contributions

AR: methodology, investigation, conceptualization, data curation, validation, writing – original draft, funding acquisition. NS: formal analysis, reviewing and editing. GS, SZN, KK: resources. KS, LSM: supervision, editing and critical revision.

Data availability

The datasets generatedduring and/or analyzed during the current study are available from thecorresponding author on reasonable request.

Declarations

Conflict of interest The authors declare that they have no conflicts to declare.

References

1. S.K. Balasingam, K. Sivalingam Nallathambi, M.H. Abdul Jabbar, A. Ramadoss, S.K. Kamaraj, M. Kundu, J. Nanomater. **209**, 1089842 (2019). https://doi.org/10.1155/2019/1089842
2. G. Karunakaran, G. Maduraiveeran, E. Kolesnikov, S.K. Balasingam, D. Kuznetsov, M. Kundu, J. Alloy. Compd. **865**, 158769 (2021). https://doi.org/10.1016/j.jallcom.2021.158769
3. A. Chaichi, G. Venugopalan, R. Devireddy, C. Arges, ACS Appl. Energy Mater. **3**, 5693 (2020). https://doi.org/10.1021/acsaem.0c00636
4. C.-R. Chen, H. Qin, H.-P. Cong, S.-H. Yu, Adv. Mater. **31**, 1900573 (2019). https://doi.org/10.1002/adma.201900573
5. Y. Zhang, H. Mei, Y. Cao et al., Coord. Chem. Rev. **438**, 213910 (2021). https://doi.org/10.1016/j.ccr.2021.213910
6. Y. Ko, M. Kwon, W.K. Bae, B. Lee, S.W. Lee, J. Cho, Nat. Commun. **8**, 536 (2017). https://doi.org/10.1038/s41467-017-00550-3
7. D. Ruan, R. Lin, K. Jiang et al., ACS Appl. Mater. Interfaces **9**, 29699 (2017). https://doi.org/10.1021/acsami.7b07522
8. R.L. Porto, R. Frappier, J.B. Ducros et al., Electrochim. Acta **82**, 257 (2012). https://doi.org/10.1016/j.electacta.2012.05.032
9. M.F. El-Kady, V. Strong, S. Dubin, R.B. Kaner, Science **335**, 1326 (2012). https://doi.org/10.1126/science.1216744
10. Y. Yue, P. Han, X. He et al., J. Mater. Chem. **22**, 4938 (2012). https://doi.org/10.1039/C2JM16128A
11. H. Zhang, Y. Chen, W. Wang et al., J. Mater. Chem. A **1**, 8593 (2013). https://doi.org/10.1039/C3TA11152K
12. M.-S. Balogun, W. Qiu, W. Wang, P. Fang, X. Lu, Y. Tong, J. Mater. Chem. A **3**, 1364 (2015). https://doi.org/10.1039/C4TA05565A
13. S. Dong, X. Chen, X. Zhang, G. Cui, Coord. Chem. Rev. **257**, 1946 (2013). https://doi.org/10.1016/j.ccr.2012.12.012
14. Y. Liu, Y. Shen, L. Sun et al., Nat. Commun. **7**, 10921 (2016). https://doi.org/10.1038/ncomms10921
15. J. Zhou, J. Lian, L. Hou et al., Nat. Commun. **6**, 8503 (2015). https://doi.org/10.1038/ncomms9503
16. C.Q. Sun, Nanoscale **2**, 1930 (2010). https://doi.org/10.1039/C0NR00245C
17. Y. Meng, D. Voiry, A. Goswami et al., J. Am. Chem. Soc. **136**, 13554 (2014). https://doi.org/10.1021/ja507463w

18. H. Kuzhandaivel, S. Manickam, S.K. Balasingam, M.C. Franklin, H.-J. Kim, KS Nallathambi, New J. Chem. **45**, 4101 (2021). https://doi.org/10.1039/D1NJ00038A

19. G. Karunakaran, G. Maduraiveeran, E. Kolesnikov et al., JOM **70**, 1416 (2018). https://doi.org/10.1007/s11837-018-2888-y

20. T.-T. Chen, H.-P. Liu, Y.-J. Wei et al., Nanoscale **6**, 5106 (2014). https://doi.org/10.1039/C4NR00101J

21. A. Fuertes, Mater. Horiz. **2**, 453 (2015). https://doi.org/10.1039/C5MH00046G

22. J. Jiang, Y. Li, J. Liu, X. Huang, C. Yuan, X.W. Lou, Adv. Mater. **24**, 5166 (2012). https://doi.org/10.1002/adma.201202146

23. H. Han, T. Song, J.-Y. Bae, L.F. Nazar, H. Kim, U. Paik, Energy Environ. Sci. **4**, 4532 (2011). https://doi.org/10.1039/C1EE02333K

24. V. Augustyn, P. Simon, B. Dunn, Energy Environ. Sci. **7**, 1597 (2014). https://doi.org/10.1039/C3EE44164D

25. E.J. Lee, L. Lee, M.A. Abbas, Phys. Chem. Chem. Phys. **19**, 21140 (2017). https://doi.org/10.1039/C7CP03546B

26. L. Yan, G. Chen, S. Tan et al., ACS Appl. Mater. Interfaces. **7**, 24212 (2015). https://doi.org/10.1021/acsami.5b07630

27. A. Ramadoss, K.-N. Kang, H.-J. Ahn, S.-I. Kim, S.-T. Ryu, J.-H. Jang, J. Mater. Chem. A **4**, 4718 (2016). https://doi.org/10.1039/C5TA10781D

28. N.R. Mucha, J. Som, J. Choi et al., ACS Appl. Energy Mater. **3**, 8366 (2020). https://doi.org/10.1021/acsaem.0c00988

29. P. Khwansungnoen, S. Chaiyakun, T. Rattana, Thin Solid Films **711**, 138269 (2020). https://doi.org/10.1016/j.tsf.2020.138269

30. J.B. Yoo, H.J. Yoo, H.J. Jung et al., J. Mater. Chem. A **4**, 869 (2016). https://doi.org/10.1039/C5TA06758H

31. M. Drygaś, C. Czosnek, R.T. Paine, J.F. Janik, Chem. Mater. **18**, 3122 (2006). https://doi.org/10.1021/cm060522z

32. B. Zhang, C. Zhang, H. He, Y. Yu, L. Wang, J. Zhang, Chem. Mater. **22**, 4056 (2010). https://doi.org/10.1021/cm101058y

33. G. Mangamma, P.K. Ajikumar, R. Nithya et al., J. Phys. D: Appl. Phys. **40**, 4597 (2007). https://doi.org/10.1088/0022-3727/40/15/035

34. N.R. Mucha, J. Som, S. Shaji et al., J. Mater. Sci. **55**, 5123 (2020). https://doi.org/10.1007/s10853-019-04278-x

35. J. Zhang, T.P. Chen, X.D. Li, Y.C. Liu, Y. Liu, H.Y. Yang, Opt. Mater. Express **6**, 2422 (2016). https://doi.org/10.1364/OME.6.002422

36. J.-C. Hsu, Y.-H. Lin, P.W. Wang, Coatings **10**, 47 (2020). https://doi.org/10.3390/coatings10010047

37. K.-N. Kang, I.-H. Kim, A. Ramadoss, S.-I. Kim, J.-C. Yoon, J.-H. Jang, Phys. Chem. Chem. Phys. **20**, 719 (2018). https://doi.org/10.1039/C7CP07473E

38. A. Achour, R.L. Porto, M.-A. Soussou et al., J. Power Sources **300**, 525 (2015). https://doi.org/10.1016/j.jpowsour.2015.09.012

39. T. Zheng, M.H. Tahmasebi, B. Li et al., ChemElectroChem **5**, 2199 (2018). https://doi.org/10.1002/celc.201800467

40. B. Wei, F. Ming, H. Liang, Z. Qi, W. Hu, Z. Wang, J. Power Sources **481**, 228842 (2021). https://doi.org/10.1016/j.jpowsour.2020.228842

41. R. Lucio-Porto, S. Bouhtiyya, J.F. Pierson et al., Electrochim. Acta **141**, 203 (2014). https://doi.org/10.1016/j.electacta.2014.07.056

42. L. Chen, C. Liu, Z. Zhang, Electrochim. Acta **245**, 237 (2017). https://doi.org/10.1016/j.electacta.2017.05.102

43. B. Gao, X. Xiao, J. Su et al., Appl. Surf. Sci. **383**, 57 (2016). https://doi.org/10.1016/j.apsusc.2016.04.173

44. B. Wei, G. Mei, H. Liang et al., J. Power Sources **385**, 39 (2018). https://doi.org/10.1016/j.jpowsour.2018.03.023